Clay Minerals (2026), 1–15
doi:10.1180/clm.2026.10025

Article

Ammonium recovery from different digestates using chabazite-rich tuff: towards scalable farm applications

Matteo Alberghini[1], Giulio Galamini[2], Cristina Botezatu[1], Barbara Faccini[1] and Giacomo Ferretti[3]

[1]Department of Environmental and Prevention Science, University of Ferrara, Ferrara, Italy; [2]Department of Chemical and Geological Sciences, University of Modena and Reggio Emilia, Modena, Italy and [3]Department of Chemical, Pharmaceutical and Agricultural Sciences, University of Ferrara, Ferrara, Italy

Abstract

The circular recovery and reuse of nutrients from wastewater is vital for achieving sustainability goals and the European Green Deal objectives. This study investigates the selective recovery of ammonium (NH_4^+) using a zeolitic tuff rich in chabazite zeolite. We focused on targeting its applicability for farm-scale applications from different anaerobic digestates undergoing various pre-treatments (screw compression, microfiltration and centrifugation). The results were compared with a zeolitic tuff rich in phillipsite and chabazite from a previous study. The tested wastewaters included swine, cattle and municipal solid waste digestates. Adsorption isotherms and kinetics were evaluated, considering key factors such as initial NH_4^+ concentration, contact time, competing ions (e.g. K^+), total solids content and pre-treatment strategies. The adsorption process followed the Freundlich model, indicating heterogeneous multilayer sorption, whereas the kinetic data aligned with pseudo-first-order and intraparticle diffusion models. NH_4^+ removal efficiency was inversely correlated with K^+ levels and solids content, with livestock-derived digestates enabling the greatest nitrogen recovery per gram of zeolitic tuff due to their favourable composition and kinetics. Among the tested pre-treatments, centrifugation proved most effective, improving active site accessibility. A preliminary field-scale trial using microfiltered swine digestate at a 3% solid-to-liquid ratio demonstrated the feasibility of batch operation, with an estimated nitrogen recovery of 715 kg N $year^{-1}$. This work lays the foundation for future comparisons with other zeolitic tuffs, such as those rich in clinoptilolite, and it supports the principle of nutrient circularity in agriculture by reducing reliance on synthetic fertilizers.

Keywords: Ammonium adsorption; chabazite; N-loaded zeolite; nutrient recycling; wastewater treatment

(Received 19 September 2025; revised 12 February 2026; Accepted Manuscript published online: 7 March 2026; Editor: George Christidis)

Nitrogen is one of the fundamental elements for crop growth and is therefore essential to meet the increasing food demand linked to population growth (FAO, 2009; Pan *et al.*, 2019). It is supplied to the soil through the application of chemical fertilizers, such as urea, or organic fertilizers. However, the industrial processes required for the production of synthetic fertilizers are no longer sustainable, as they require high energy consumption and release large amounts of greenhouse gases to the atmosphere (Pesendorfer & Ellersdorfer, 2021). Moreover, once applied to agricultural soils, synthetic fertilizers release nutrients rapidly, often resulting in low use efficiency by crops and the consequent release of large amounts of nitrogen to the environment (Hooda *et al.*, 2000; Ferretti *et al.*, 2020). As an alternative to synthetic fertilizers, liquid digestates derived from the anaerobic digestion of livestock or the organic fraction of municipal solid waste (MD; i.e. municipal digestate) are often applied to sustain crop growth (Ferretti *et al.*, 2020; Kovačić *et al.*, 2022; Rossi *et al.*, 2023; Galamini *et al.*, 2025). The nutrient content of these matrices varies depending on the type of livestock and animal diet or the composition of waste (in the case of municipal solid waste wastewaters), as well as the operating conditions of anaerobic digestion plants (Makádi *et al.*, 2012). This variability makes it difficult to determine the correct fertilizer dosage to use (Pesendorfer & Ellersdorfer, 2021), increasing the risk of nutrient losses and associated negative environmental impacts, such as water eutrophication, CH_4, CO_2, N_2O and ammonia (NH_3) emissions and the release of pathogens into water bodies (Huang *et al.*, 2017; Ferretti *et al.*, 2020; Fu *et al.*, 2020; Nhubu *et al.*, 2020; Nguyen *et al.*, 2022; Policastro & Cesaro, 2023; Galamini *et al.*, 2025).

To address these issues, several regulations have been introduced by the European Union (EU), including the Nitrates Directive (91/676/EEC) in 1991 (Huygens *et al.*, 2020). Additionally, the European Green Deal objectives include: (1) reducing nitrogen concentrations in effluents and digestates; (2) limiting greenhouse gas emissions during storage and field application; and (3) preventing soil and water contamination (European Union, 1998; Martinez *et al.*, 2009; United Nations, 2015; European Commission, 2020).

Corresponding author: Giacomo Ferretti; Email: frrgcm@unife.it

Cite this article: Alberghini M, Galamini G, Botezatu C, Faccini B and Ferretti G (2026) Ammonium recovery from different digestates using chabazite-rich tuff: towards scalable farm applications. *Clay Minerals*, 1–15. https://doi.org/10.1180/clm.2026.10025

© The Author(s), 2026. Published by Cambridge University Press on behalf of The Mineralogical Society of the United Kingdom and Ireland. This is an Open Access article, distributed under the terms of the Creative Commons Attribution licence (http://creativecommons.org/licenses/by/4.0), which permits unrestricted re-use, distribution and reproduction, provided the original article is properly cited.

In this context, nutrient recovery and recycling from wastewater are crucial, as they could help save energy in production processes while reducing environmental contamination risks (Galamini *et al.*, 2023, 2025). Several technologies have been proposed for nitrogen removal from wastewater, including chemical precipitation, ammonia stripping, electrolytic methods, biological degradation and physical adsorption (Kovačić *et al.*, 2022). Among these, adsorption stands out for its versatility, low operating costs and process simplicity. Materials such as biochar (Hou *et al.*, 2016; Banik *et al.*, 2023), nanoparticles (Zare *et al.*, 2016) and natural zeolites (Faccini *et al.*, 2015; Tasić *et al.*, 2019; Galamini *et al.*, 2020) have been widely studied for their ability to adsorb ammonium (NH_4^+). Zeolites in particular are hydrated aluminosilicates with a porous three-dimensional structure composed of $[SiO_4]^{4-}$ and $[AlO_4]^{5-}$ tetrahedra, forming channels and cavities capable of hosting exchangeable cations (Coombs *et al.*, 1998; Dyer & Zubair, 1998). Their affinity for NH_4^+ depends on their crystal structure, chemical composition and any chemical treatments they have undergone (Nguyen & Tanner, 1998). Several studies have demonstrated their applicability to the removal of NH_4^+ from a large variety of wastewaters, and their application to soil also improves soil health in the long term and promotes crop growth while reducing nitrogen losses (Di Giuseppe *et al.*, 2016; Ali *et al.*, 2017; Eroglu *et al.*, 2017; Ghasemi *et al.*, 2018; Mpanga *et al.*, 2020; Cataldo *et al.*, 2021; Jarosz *et al.*, 2022; Galamini *et al.*, 2023; Ferretti *et al.*, 2024).

Most studies in this area focus on NH_4^+ adsorption from synthetic solutions (Pan *et al.*, 2019; Fu *et al.*, 2020; Pesendorfer & Ellersdorfer, 2021; Muscarella *et al.*, 2023), while few evaluate its removal efficiency using real wastewaters (Huang *et al.*, 2015; Galamini *et al.*, 2020). Moreover, existing research tends to consider a single type of wastewater, whereas a comparative analysis of different types of wastewater is still lacking.

Recently, Alberghini *et al.* (2025) evaluated the NH_4^+ adsorption performance of a zeolitic tuff composed of two distinct zeolite phases: phillipsite and chabazite. The study involved testing five anaerobic digestates originating from both livestock effluents and municipal solid waste, which had undergone various pre-treatment processes, including screw separation, microfiltration and centrifugation. The findings demonstrated the high potential of that specific tuff for efficient NH_4^+ recovery under realistic operational conditions. Moreover, the study offered a preliminary farm-scale assessment, estimating annual nitrogen recovery at between ~440 and ~6000 kg N $year^{-1}$, depending on the digestate and solid-to-liquid (S/L) ratio.

Given the wide diversity of natural zeolitic tuffs, their varying availability across different regions and the distinct properties associated with each zeolite type, further investigation is essential. To enhance both the understanding and scalability of this recovery process, detailed studies on the behaviour and performance of other commercially available zeolitic tuffs are thus necessary.

The aim of this study was therefore to broaden the characterization of commercially available materials for potential use in nutrient recycling technologies by characterizing the behaviour of another diffused zeolitic tuff across a wide spectrum of treatable matrices.

To achieve this aim, the experimental design of Alberghini *et al.* (2025) was adopted to assess the performance of a zeolitic tuff composed predominantly of chabazite (~70%) in NH_4^+ removal from three types of digestates derived from municipal solid waste, swine and cattle livestock. The study focused on the practical applicability of the chabazite-rich tuff for ammonium recovery under both laboratory and preliminary farm-scale conditions, including the effects of digestate composition, solids content, pre-treatment processes, competing ions and NH_4^+ concentrations. Adsorption isotherms and kinetics were constructed to describe the process, and the potential amounts of nitrogen recoverable on a daily and annual basis by a model farm implementing this approach were estimated, providing actionable insights to support the development of scalable nutrient recovery applications. The NH_4^+-saturated tuff produced through this process is designed for direct use as a slow-release soil amendment, being fully consistent with the objectives of the European Green Deal.

Materials and methods

Materials

The chemical characteristics of the digestates used are reported in Table 1. The cattle-derived digestate, collected from a biogas plant near San Biagio (Ferrara province, Italy), was available only after separation by screw compression process (CD-S). The swine-derived digestate was sampled from a swine livestock near Formigine (Modena province, Italy) and was analysed in two different forms: after separation by screw compression (SD-S) and after microfiltration (SD-M). This latter process consisted of a microfiltration step after the screw compression using a 40 MFT SAVECO filter from WAM Group S.p.A. (Modena province, Italy). The MD-derived digestates were collected from an anaerobic digestion plant near Spilamberto (Modena province, Italy). These were available in two fractions: the raw digestate (MD-R), corresponding to the liquid fraction leaving the digester, and the clarified digestate (MD-C), obtained through a centrifugation process aimed at reducing suspended solids.

All digestates exhibited a high concentration of NH_4^+-N and total solids (TS), with particularly elevated values observed in those derived from livestock manure. The cattle digestate (CD-S) also showed a notably high potassium (K^+) content.

The zeolitic tuff used is a chabazite-rich tuff extracted from central Italy. The material belongs to the Lithic Yellow Tuff (Sorano Formation) and is part of the Latera Volcanic Complex, a stratigraphic sequence primarily composed of pyroclastic deposits (Vezzoli *et al.*, 1987). This material is the same as that employed in many previous studies (Di Giuseppe *et al.*, 2016; Galamini *et al.*, 2023, 2024, 2025; Ferretti *et al.*, 2024). The tuff was quarried from the 'Piandirena' site, an area of ~60,000 m^2 near Sorano (Grosseto province, Italy), located at ~450 m above sea level (42°41′26.52″N, 11°44′35.54″E), and it was provided by Verdi S.p.A. company (Reggio Emilia, Italy). The mineralogical composition of the zeolitic tuff is listed in Table 2. The cation-exchange capacity (CEC) previously determined by Malferrari *et al.* (2013) is 217 cmol kg^{-1}, with Ca^{2+} being the prevalent exchangeable cation (146 cmol kg^{-1}), followed by K^+ (60 cmol kg^{-1}), Na^+ (7 cmol kg^{-1}) and Mg^{2+} (4 cmol kg^{-1}). The particle-size distribution of the tuff was determined using the sequential sieving method as follows: 12.5% between 5 and 2 mm, 60.4% between 2 and 0.8 mm, 24.1% between 0.8 and 0.425 mm and 3.0% below 0.425 mm. Prior to the experiments, the zeolitic tuff was repeatedly rinsed with Type I ultrapure water (18.2 MΩ cm^{-1} at 25°C) and dried at 105°C for 48 h to remove gravimetric water.

Table 1. Physicochemical properties of the digestates. Values are expressed as mean ± standard deviation, based on three replicates.

Property	Unit	MD-R	MD-C	SD-S	SD-M	CD-S
pH		7.89 ± 0.05	8.66 ± 0.00	7.62 ± 0.01	7.77 ± 0.00	7.75 ± 0.01
EC	mS cm^{-1}	25.8 ± 0.4	21.7 ± 0.5	27.4 ± 1.5	27.2 ± 0.7	35.8 ± 1.5
TS	g L^{-1}	14.1 ± 2.0	8.3 ± 0.1	32 ± 0.2	28.6 ± 0.4	31.6 ± 1.9
TKN	mg L^{-1}	2514 ± 12	1812 ± 22	4353 ± 190	4100 ± 117	3950 ± 79
NH_4^+-N	mg L^{-1}	2031 ± 24	1681 ± 37	3085 ± 156	2993 ± 150	3000 ± 91
Na^+	mg L^{-1}	1474 ± 90	2010 ± 47	557 ± 36	558 ± 32	285 ± 41
Mg^{2+}	mg L^{-1}	188 ± 51	102 ± 7	275 ± 34	161 ± 1	129 ± 12
K^+	mg L^{-1}	1799 ± 125	1587 ± 32	2044 ± 104	2115 ± 81	4326 ± 328
Ca^{2+}	mg L^{-1}	1414 ± 412	77.4 ± 19.7	720 ± 41	725 ± 24	293 ± 47

EC = electrical conductivity; TKN = total Kjeldahl nitrogen.

Table 2. The zeolitic tuff characteristics. Chemical composition data were obtained through X-ray fluorescence analysis.

Chemical composition	%	QPA	%
SiO_2	56.9	Chabazite	68.5
TiO_2	0.51	Phillipsite	1.8
Al_2O_3	16.8	Analcime	0.6
Fe_2O_3	3.42	K-feldspar	9.7
MnO	0.10	Mica	5.3
MgO	1.79	Pyroxene	2.9
CaO	4.91	Volcanic glass	11.2
Na_2O	0.63		
K_2O	5.64	TZC	70.9
P_2O_5	0.21		
LOI	8.97		

LOI = loss on ignition; QPA = quantitative phase analysis; TZC = total zeolitic content.

Methods

Batch adsorption experiment

From an industrial perspective, it is important to evaluate the NH_4^+ sorption efficiency of the adsorbent by studying both adsorption isotherm and kinetics. Isotherms describe the equilibrium between adsorption and desorption at thermodynamic equilibrium and are useful for optimizing a process, particularly for determining the amount of adsorbent required to achieve a specific removal efficiency. Kinetics, on the other hand, are useful to define the ideal contact time between the digestate and the zeolitic tuff needed to reach the desired removal efficiency.

The NH_4^+ removal efficiency (R_E%) of the zeolitic tuff was determined using Equation 1 (Detho *et al.*, 2023), whereas the amount of NH_4^+ adsorbed at equilibrium (q_e; mg g^{-1}) was determined using Equation 2 (Fu *et al.*, 2020):

$$R_E\,(\%) = \frac{(C_0 - C_e)}{C_0} \times 100 \quad (1)$$

where C_0 (mg L^{-1}) is the initial NH_4^+ concentration and C_e (mg L^{-1}) is the equilibrium concentration; and

$$q_e = \frac{(C_0 - (C_0 - C_b) - C_e) \times V}{m} \quad (2)$$

where C_0 (mg L^{-1}) is the initial NH_4^+ concentration, C_b (mg L^{-1}) is the NH_4^+ concentration in blanks after 24 h, C_e (mg L^{-1}) is the concentration at equilibrium, V (L) is the volume of digestate and m (g) is the mass of zeolitic tuff. Blank samples without zeolitic tuff were considered to assess the possible effects of ammonia stripping or NH_4^+ adsorption on the surface of the plastic containers.

Isotherms were generated at 25°C using 12 different S/L ratios, expressed as mass of zeolitic tuff per volume of digestate (w/v%). These ratios ranged from 1% to 50%, meaning that variable amounts of zeolitic tuff (0.8–40 g) were added to 80 mL of digestate in 100 mL sealed plastic bottles, which were shaken at 200 rpm for 24 h (assumed equilibrium time). After shaking, the NH_4^+ concentration in the liquid phase was measured immediately. According to previous studies, zeolite adsorption of NH_4^+ remains constant within a pH range of 2–8 but declines significantly at pH values above 9 (Galamini *et al.*, 2020; Guo *et al.*, 2008). Given that the pH of all tested digestates ranged between 7.7 and 8.5, pH variation was not specifically investigated so as to avoid additional chemical inputs.

Kinetic experiments

Kinetic adsorption models of NH_4^+ onto zeolitic tuff were determined for each digestate. A fixed amount of zeolitic tuff corresponding to 5% S/L ratio (w/v) was added (i.e. 25 g of zeolitic tuff in 500 mL of each digestate), and the suspensions were shaken in an orbital shaker at 25°C and 200 rpm for 420 min. At 12 time intervals, corresponding to 5, 10, 15, 20, 30, 45, 60, 90, 120, 180, 360 and 420 min, 10 mL aliquots were sampled and immediately analysed for NH_4^+ concentration. The progressive volume reduction due to sampling was considered in the subsequent calculations of adsorption capacity over time. The amount of NH_4^+ adsorbed at any time (q_t; mg g^{-1}) was determined using Equation 2, substituting q_e and C_e with q_t and C_t, respectively.

Isotherm and kinetic models

Several isotherm models have been proposed in the literature to describe the equilibrium adsorption of NH_4^+ (Wasielewski *et al.*, 2018; Fu *et al.*, 2020; Galamini *et al.*, 2020; Eberle *et al.*, 2022; Muscarella *et al.*, 2023; Zhou *et al.*, 2024). Among these, the Langmuir and Freundlich models are frequently identified as the most suitable for describing NH_4^+ adsorption on natural zeolites. Consequently, these models were selected in this study as well.

The isotherm data were processed using *RStudio* (version 2023-3.0-386; R Core Team, 2021) with the *PUPAIM* package (version 0.3.1; Deocaris & De Osio, 2020). Model performance was assessed based on the coefficient of determination (R^2), Akaike information criterion (AIC) and p-value. As highlighted by Wang & Guo (2020a), nonlinear models provide more accurate parameter estimations. Therefore, the parameters of the Langmuir and Freundlich models were determined using their nonlinear formulations.

The Freundlich adsorption isotherm describes multilayer adsorption on heterogeneous surfaces, where adsorption is non-ideal and reversible (Freundlich, 1906). It follows Equation 3:

$$q_e = K_F C_e^{1/n} \quad (3)$$

where q_e is the equilibrium adsorption capacity (mg g^{-1}), K_F is the Freundlich constant, C_e the equilibrium concentration (mg L^{-1}) and n is an empirical parameter related to adsorption intensity.

The Langmuir isotherm assumes monolayer adsorption on homogeneous sites, meaning each site can hold only one adsorbate molecule, with no interactions occurring between them (Wang & Guo, 2020a). It follows Equation 4:

$$q_e = \frac{q_{max} K_L C_e}{1 + K_L C_e} \quad (4)$$

where q_e is the equilibrium adsorption capacity (mg g^{-1}), q_{max} represents the maximum adsorption capacity (mg g^{-1}), C_e is the concentration at equilibrium (mg L^{-1}) and K_L is the Langmuir constant (L mg^{-1}). Adsorption favourability is assessed *via* the separation factor R_L (Weber & Chakravorti, 1974), calculated using Equation 5:

$$R_L = \frac{1}{1 + K_L C_0} \quad (5)$$

where C_0 is the initial concentration. Adsorption is favourable when $0 < R_L < 1$, unfavourable if $R_L > 1$, linear if $R_L = 1$ and irreversible if $R_L = 0$.

The spontaneity of adsorption is evaluated through the Gibbs free energy ($\Delta G°$), calculated using Equation 6 (Jha & Hayashi, 2009):

$$\Delta G^\circ = -RT\ln(K_e) \quad (6)$$

where R is the gas constant (8.314 J $mol^{-1}\cdot K^{-1}$), T is the absolute temperature and K_e is the thermodynamic equilibrium constant. K_e is determined by extrapolating the intercept in a plot of q_e/C_e *vs* C_e as C_e approaches zero (Khan & Singh, 1987). A negative $\Delta G°$ indicates a spontaneous and energetically favourable adsorption process.

Several kinetic models have been used in the past to describe the adsorption of NH_4^+ onto zeolitic tuff, including the pseudo-first-order (PFO), pseudo-second-order (PSO) and Elovich models (Wen *et al.*, 2006; Pan *et al.*, 2019; Galamini *et al.*, 2020; Damodara & Parameswaran, 2021; Duyen *et al.*, 2022; Eberle *et al.*, 2022). However, the PFO and PSO models are generally more efficient at fitting experimental data; therefore, they were selected for this study. Adsorption kinetics should be analysed using data far from equilibrium (Simonin, 2016). Therefore, only data with a fractional uptake $F(t) \leq 0.90$ were considered.

Experimental data was processed using *RStudio* (version 2023-3.0-386) and the *PUPAK* package (version 0.1.1; Magalong *et al.*, 2022). The best-fitting kinetic model was assessed based on statistical parameters, including the root mean square error (RMSE), mean square error (MSE), AIC and Bayesian information criterion (BIC), where lower values indicate a better fit.

The nonlinear PFO model, proposed by Lagergen (1898), is described by Equation 7:

$$q_t = q_e(1 - e^{k_1 t}) \quad (7)$$

where q_e and q_t represent the adsorption capacity at equilibrium and at time t (mg g^{-1}), respectively, while k_1 is the PFO rate constant (min^{-1}).

The nonlinear form of the PSO model is given by Equation 8:

$$q_t = \frac{(q_e)^2 k_2 t}{1 + q_e k_2 t} \quad (8)$$

where q_e and q_t represent the adsorption capacity at equilibrium and at time t (mg g^{-1}), respectively, while k_2 is the PSO rate constant (g mg^{-1} min^{-1}).

As the PFO and PSO models do not provide insights into the diffusion mechanism of NH_4^+, the Intraparticle Diffusion (ID) model (Weber *et al.*, 1963), described by Equation 9, was applied to the experimental data:

$$q_t = k_{ID} t^{0.5} + C \quad (9)$$

where q_t (mg g^{-1}) is adsorption capacity at time t (min), k_{ID} (mg g^{-1} $min^{0.5}$) is the ID rate constant and C is the intercept of the slope of the curve, which is also indicative of the boundary-layer thickness. If the plot of q_t *vs* $t^{0.5}$ intercepts the origin ($C \approx 0$), ID is considered to be the rate-controlling step (Wasielewski *et al.*, 2018). The presence of multiple linear regions in a plot suggests a multi-stage adsorption process, with the first region corresponding to surface adsorption or macropore diffusion (Halim *et al.*, 2010; Widiastuti *et al.*, 2011).

Model-based calculation of nitrogen recovery from digestates

To evaluate the amount of nitrogen recovery at the farm scale, a theoretical calculation was performed based on the average daily volume of digestate produced per biogas plant, which, based on the national reports, was assessed to be 10 m^3 per day (Dal Verme *et al.*, 2021; European Biogas Association, 2022). Based on this data, the amount of N recoverable per cycle was calculated using Equation 10, and the amount of N recoverable yearly was calculated using Equation 11:

$$\text{kg N recovered per cycle} = q_e \times \text{kg zeolite per cycle} \quad (10)$$

$$\text{kg N recovered year} = \text{kg N recovered per cycle} \times \text{number of cycles} \times 365 \quad (11)$$

The duration of each treatment cycle, representing the time during which fresh digestate is in contact with the zeolitic tuff, was calculated by considering both the time required to reach equilibrium in the kinetic experiments and the additional time needed for loading and unloading the pilot-scale prototype, estimated as 20 min before and after the equilibrium contact time. The number of cycles was then derived assuming continuous plant operation, with the S/L ratio and the amount of NH_4^+ adsorbed at equilibrium (q_e) corresponding to the optimal values identified in the experimental trials.

Analytical techniques

Electrical conductivity (EC) was determined in digestate samples diluted 1:10 (w/v) using an RS 180-7127 probe (Hanna Instrument, Woonsocket, RI, USA), while pH measurements were performed on undiluted samples with an electrode connected to an 877 Titrino plus automatic titration unit (Methrom, Origgio, Italy). Total Kjeldahl nitrogen (TKN) was quantified after digesting the samples with 98% H_2SO_4 and catalyst tablets containing TiO_2, $CuSO_4$ and K_2SO_4 using an IR Digester K-425 (Büchi, Flawil, Switzerland). The digested samples were then distilled with a K-360 unit (Büchi, Flawil, Switzerland), employing a 4% H_3BO_3 acid

trap pre-buffered at pH 4.65 ± 0.01 to capture the released NH_3. NH_4^+ was subsequently determined by endpoint titration with 0.25 M H_2SO_4 using the 877 Titrino plus automatic titration unit (Methrom, Origgio, Italy). NH_4^+ concentration was measured by directly distilling the samples, bypassing the digestion step. The concentrations of major cations (Na^+, K^+, Ca^{2+} and Mg^{2+}) in the digestates were analysed using inductively coupled plasma mass spectrometry (ICP-MS) with a Thermo Electron Corporation X Series mass spectrometer (Thermo Fisher Scientific, Bremen, Germany). Samples were pre-diluted 1:500, filtered through 0.45 µm polytetrafluoroethylene (PTFE) syringe filters and stabilized with 2% HNO_3 to maintain pH < 2. TS content was determined by measuring the weight change of a known sample volume after drying overnight at 105°C. The chemical composition of the zeolitic tuff was assessed through X-ray fluorescence (XRF) analysis on powder pellets using a wavelength-dispersive ARL Advant'X spectrometer (Thermo Scientific, Waltham, MA, USA). The estimated accuracy and precision are within 3% for major elements such as Si, Ti, Fe, Ca and K and within 7% for Mg, Al, Mn and Na; for trace elements (above 10 ppm), both accuracy and precision remain below 10%.

The mineralogical characterization of the zeolitic tuff was performed using X-ray powder diffraction (XRPD) with an X'Pert PRO modular powder diffractometer (PANalytical, Malvern, UK). To minimize preferred crystallite orientations, the zeolitic tuff was back-loaded. The amorphous phase content was quantified by adding 20% (w/w) ZnO to the sample. Rietveld refinements and quantitative phase analyses were conducted using the fundamental parameters approach implemented in *Profex–BGMN* (version 5.0.1; Cheary *et al.*, 2004), with crystal structures sourced from the *BGMN* database.

Results and discussion

Ammonium removal kinetics

Figure 1 shows the kinetics of NH_4^+ adsorption up to 420 min. NH_4^+ adsorption showed a relatively fast initial uptake. The equilibrium stage was attained after 120 min for MD-R and MD-C and within 90 min for SD-S, SD-M and CD-S. The high amount of NH_4^+ adsorbed by the zeolitic tuff at the beginning of the experiment could be attributed to both the greater availability of negatively charged surface sites and the presence of extra-framework sites available for ion exchange during the early stages of the adsorption process (Sánchez-Hernández *et al.*, 2018; Wang & Guo 2020b; Vamvuka *et al.*, 2024). A cation may either adsorb onto the external surface of the channels or exchange with the cations originally occupying the zeolitic cages (Chen *et al.*, 2018). However, a detailed investigation of the precise location and distribution of NH_4^+ within the zeolite framework is beyond the scope of this study, which focuses on evaluating the overall adsorption performance under practical conditions. As the adsorption process continued, the number of available sites decreased, and it approached zero at equilibrium. The differences in the time required to reach equilibrium between the different digestates could be due to the different initial NH_4^+ concentrations. An increase in NH_4^+ concentration may enhance the saturation rate of exchange sites, thereby promoting a more rapid establishment of the adsorption equilibrium. Several others studies reported a similar trend (Huang *et al.*, 2010, 2015; Cheng & Ding, 2015; Kotoulas *et al.*, 2019; Galamini *et al.*, 2020; Tang *et al.*, 2020; Damodara & Parameswaran, 2021; Liu, *et al.*, 2022; Susilawati *et al.*, 2025). For example, Huang *et al.* (2010) found that the amount of NH_4^+ adsorbed increased very quickly within the first 60 min to reach the equilibrium stage after 120 min. In addition, Damodara & Parameswaran (2021) and Kotoulas *et al.* (2019) observed a rapid increase in the amount of NH_4^+ adsorbed by a zeolitic tuff in the early stages of the adsorption process and the attainment of equilibrium after 90–120 min. These aspects are critical for process optimization at the real-world scale, particularly in terms of energy consumption, processing time and overall cost efficiency, as faster attainment of equilibrium enables shorter contact times and reduces equipment operational time.

Given the importance of kinetic analysis for designing processes in water treatment applications, the adsorption kinetics were assessed through nonlinear regression by fitting the PFO and PSO models (Fig. 1).

The PFO model provided a better fit than the PSO model for all types of digestate (Fig. 1 & Table 3). This is at odds with most previous works on NH_4^+ adsorption onto zeolitic tuffs, where the PSO model typically offers a better representation of the kinetic data (Halim *et al.*, 2010; Huang *et al.*, 2010; Moussavi *et al.*, 2011; Widiastuti *et al.*, 2011; Wasielewski *et al.*, 2018; Tang *et al.*, 2020; Damodara & Parameswaran, 2021). However, this study is in agreement with Sánchez-Hernández *et al.* (2018), who also observed a better fit with the PFO model under specific experimental conditions. In previous studies, all kinetic data points were considered during modelling. However, including data points close to the equilibrium may mask the actual adsorption behaviour, often leading to a better fit with models such as the PSO model, even when they may not be the most representative (Simonin, 2016). In contrast, focusing on the earlier stages of adsorption (i.e. data farther from the equilibrium) can sometimes reveal a better fit with models such as the PFO model, as observed in this study and in Sánchez-Hernández *et al.* (2018). In fact, the PSO equation often provides a good fit at the equilibrium stage but may not accurately describe the adsorption process across the entire time range (Ho & Mckay, 1998). The PFO model describes the NH_4^+ removal kinetics where the rate of removal is initially fast and proportional to the remaining amount to be removed, then decreasing as equilibrium is approached. This behaviour, which is typical of many adsorbent systems including zeolitic materials, is well described by the PFO model, which empirically represents processes often governed by surface diffusion or external control. The kinetic parameters, including k_1 and k_2, were determined using the *PUPAK* tool. k_1 in particular provides insights into how rapidly the system approaches equilibrium (Plazinski *et al.*, 2009). In our study, k_1 decreased as the NH_4^+ concentration increased, implying a greater driving force that accelerates adsorption, particularly in the initial stages (Taddeo *et al.*, 2017). However, plotting the PSO and PFO models alone is insufficient to fully describe the kinetics of adsorption. Therefore, the ID model was also applied to explore the diffusion mechanism of NH_4^+. Figure 2 & Table 4 show the q_t *vs* $t^{0.5}$ plots and the corresponding ID model parameters, respectively.

In agreement with several previous studies (Huang *et al.*, 2015; Galamini *et al.*, 2020; Damodara & Parameswaran, 2021; Susilawati *et al.*, 2025), the q_t *vs* $t^{0.5}$ plots did not pass through the origin, indicating that ID contributed to NH_4^+ removal but was not the only process affecting the adsorption rate. Three distinct linear regions were observed in all q_t *vs* $t^{0.5}$ plots. The first region represents the initial stage of adsorption, where rapid uptake is attributed to external surface adsorption or instantaneous ion exchange. This phase

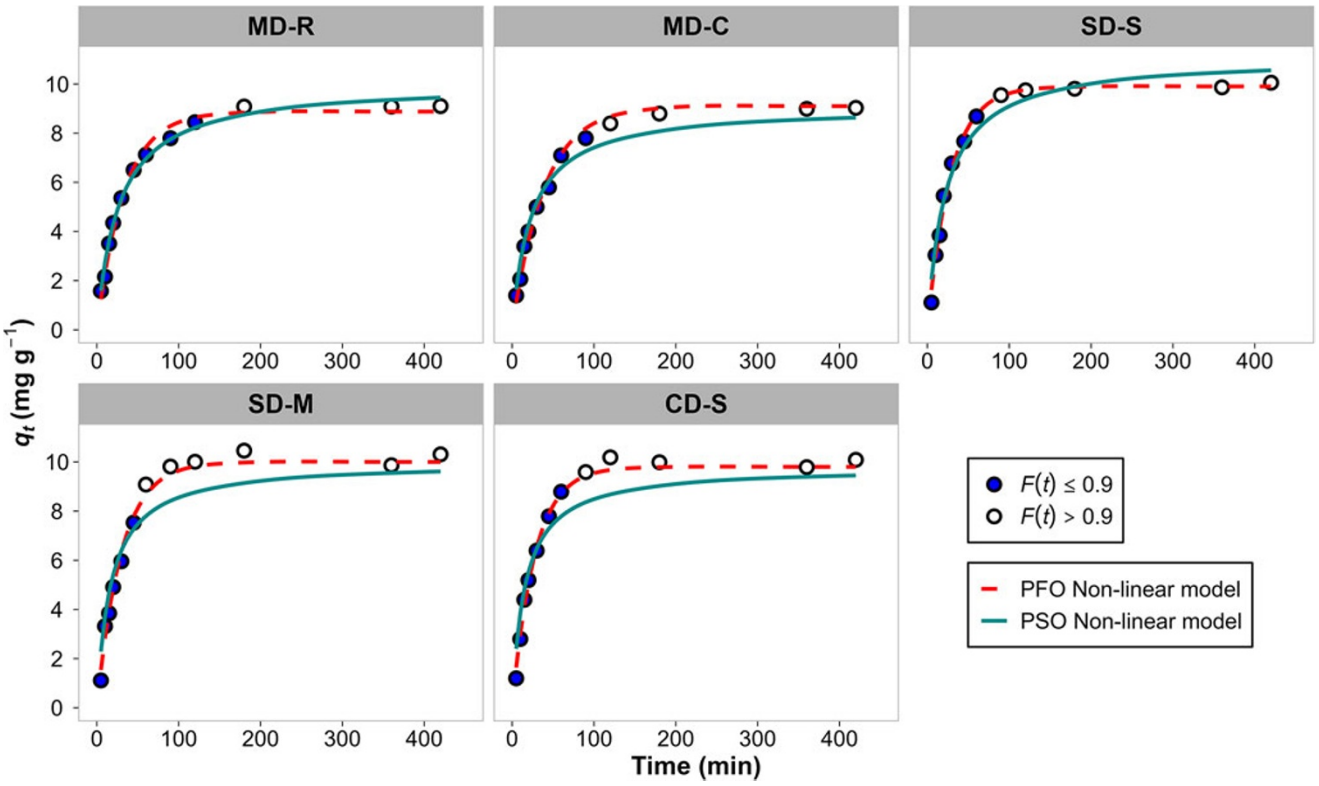

Figure 1. Kinetics of NH_4^+ adsorption for the different digestates; data with $F(t) \leq 90\%$ have been considered in kinetic analyses; data with $F(t) > 90\%$ were not taken into consideration.

Table 3. Statistical and kinetic parameters of the tested PSO and PFO models.

Digestate	Model	RMSE	MSE	AIC	BIC	k_1 (min^{-1})	k_2 (g mg^{-1} min^{-1})
MD-R	PFO	0.4	0.1	10.7	11.1	0.027	
	PSO	0.4	0.2	14.1	14.5		0.004
MD-C	PFO	0.3	0.1	8.4	8.6	0.026	
	PSO	0.4	0.1	11.4	11.6		0.005
SD-S	PFO	0.3	0.1	7.4	7.0	0.036	
	PSO	0.6	0.4	15.7	15.2		0.005
SD-M	PFO	0.3	0.1	6.7	6.3	0.032	
	PSO	0.5	0.2	11.8	11.4		0.005
CD-S	PFO	0.2	0.0	2.8	0.7	0.036	
	PSO	0.7	0.5	19.2	19.1		0.006

was particularly short for digestates with greater initial NH_4^+ concentrations, such as those of livestock origin, confirming a strong initial driving force. The second region corresponds to the gradual adsorption phase, where ID contributes to a slower uptake (Hou *et al.*, 2016). The adsorption rate constant for the first region (k_{ID1}) is consistently higher than that of the second region (k_{ID2}), and the diffusion boundary-layer thickness in region 2 (C_2) is larger than in region 1 (C_1) for all digestates (Table 4). This indicates that the removal efficiency was initially greater due to the abundance of available exchange sites and greater surface accessibility (Zhou *et al.*, 2024). As adsorption progressed, a boundary layer formed due to interactions between the zeolitic surface and NH_4^+ ions. Once external sites were saturated, further uptake depended on the diffusion of ions into the internal structure of the adsorbent. However, the non-zero intercepts of the q_t *vs* $t^{0.5}$ plots confirm that ID was not the sole process involved (Karaçetin *et al.*, 2014). Finally, the third region reflects the equilibrium phase, in which all active sites are saturated and the adsorbent attains maximum capacity (Damodara & Parameswaran, 2021).

Effects of the S/L ratio and digestate properties

As expected, increasing the S/L ratio led to greater removal efficiency but simultaneously to lower q_e values (Fig. 3a,b) because a larger mass of zeolitic tuff provides more exchangeable sites, allowing for a greater total amount of NH_4^+ to be removed from the digestate (Sánchez-Hernández *et al.*, 2018). NH_4^+ ions migrate from the digestate towards the adsorbent surface mainly due to electrostatic attraction and occupy the active adsorption sites. At lower S/L ratios, adsorption sites become saturated faster, resulting in higher q_e values, whereas at higher S/L ratios, many active sites remain unoccupied, leading to lower NH_4^+ adsorption per unit mass of zeolite (Mazloomi & Jalali, 2016; Kotoulas *et al.*, 2019). As the exchangeable sites on the zeolite surface become fully occupied,

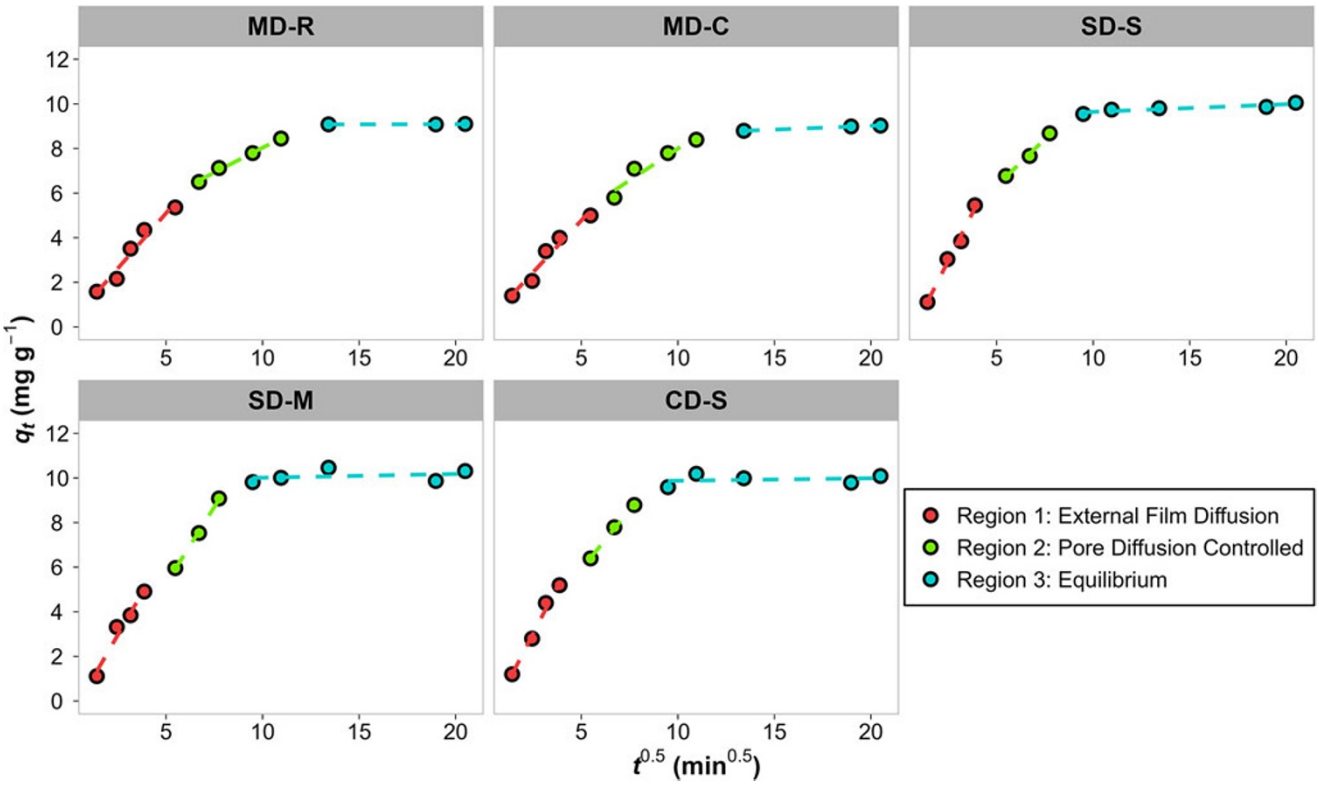

Figure 2. ID plots: amount of NH_4^+ adsorbed at any time (q_t) *vs* $t^{0.5}$ plot for the different digestates.

Table 4. ID parameters for the ID model.

Digestate	Region	k_{ID} (mg g^{-1} min$^{-0.5}$)	C (mg g^{-1})
MD-R	Region 1	1.23	−1.34
	Region 2	0.446	3.57
MD-C	Region 1	1.03	−0.857
	Region 2	0.402	3.96
SD-S	Region 1	1.94	−3.20
	Region 2	1.10	0.310
SD-M	Region 1	2.19	−3.79
	Region 2	1.27	−0.860
CD-S	Region 1	1.86	−3.02
	Region 2	0.841	2.14

equilibrium is reached, limiting further NH_4^+ removal (Susilawati *et al.*, 2025). Among the tested digestates, the removal efficiency followed the trend MD-C > MD-R > SD-S > CD-S > SD-M, highlighting a generally greater performance for digestates derived from municipal solid waste compared to those of swine or cattle origins. These findings are consistent with previous studies reporting that NH_4^+ removal efficiency tends to decrease significantly at higher S/L ratios (Huang *et al.*, 2010; Sánchez-Hernández *et al.*, 2018; Tang *et al.*, 2020; Susilawati *et al.*, 2025). Our observation is especially relevant for industrial applications, where achieving high NH_4^+ removal with minimal zeolitic tuff usage is essential to reduce operational costs and enhance process sustainability. From an industrial perspective, the use of very high S/L ratios is generally avoided, as they would entail excessive costs in terms of both the adsorbent material and operation processes. Nevertheless, it should be considered that higher adsorbent dosages are required when the objective is to maximize the reduction of the NH_4^+ concentration in the wastewater, whereas lower dosages are more suitable when the aim is to maximize the nitrogen load per unit of adsorbent.

Adsorption isotherms and fitting models

The adsorption equilibrium data were analysed using Langmuir and Freundlich isotherm models (Fig. 4), and the estimated parameters are listed on Table 5. Due to its intrinsic complexity, the adsorption process cannot be univocally defined as homogeneous or heterogeneous, nor exclusively attributed to physical or chemical interactions (Eberle *et al.*, 2022). Most previous studies applied Langmuir and Freundlich isotherm models to describe the adsorption process (Lin *et al.*, 2013; Taddeo *et al.*, 2017; Kotoulas *et al.*, 2019; Eberle *et al.*, 2022; Zhou *et al.*, 2024).

Both the Freundlich and Langmuir models adequately describe the experimental data (c.f. R^2, AIC and *p*-values; Table 5), indicating that NH_4^+ adsorption onto the zeolitic tuff occurs with both homogeneous and heterogeneous characteristics (Sánchez-Hernández *et al.*, 2018). However, among the two, the Freundlich model generally yielded slightly better fits across most experimental conditions, highlighting the multilayer and heterogeneous nature of the adsorption process. This interpretation aligns with the kinetic studies, which also indicated a complex adsorption process. Further evidence supporting the heterogeneous nature of the process is provided by the Freundlich constant $1/n$, which remained consistently below 1 across all tested digestates. Lower $1/n$ values indicate higher surface heterogeneity, consistent with adsorption occurring on sites with varying affinities (Haghseresht & Lu, 1998). In our study, $1/n$ values ranged between 0.4 and 0.6,

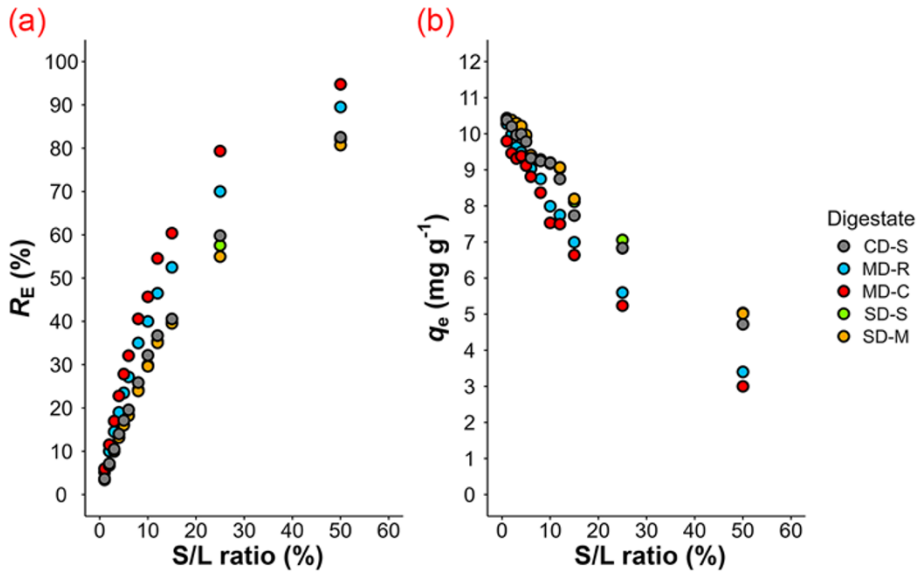

Figure 3. (a) NH_4^+ removal efficiency (R_E) as a function of the S/L ratio; (b) amount of NH_4^+ adsorbed at equilibrium (q_e) as a function of the S/L ratio.

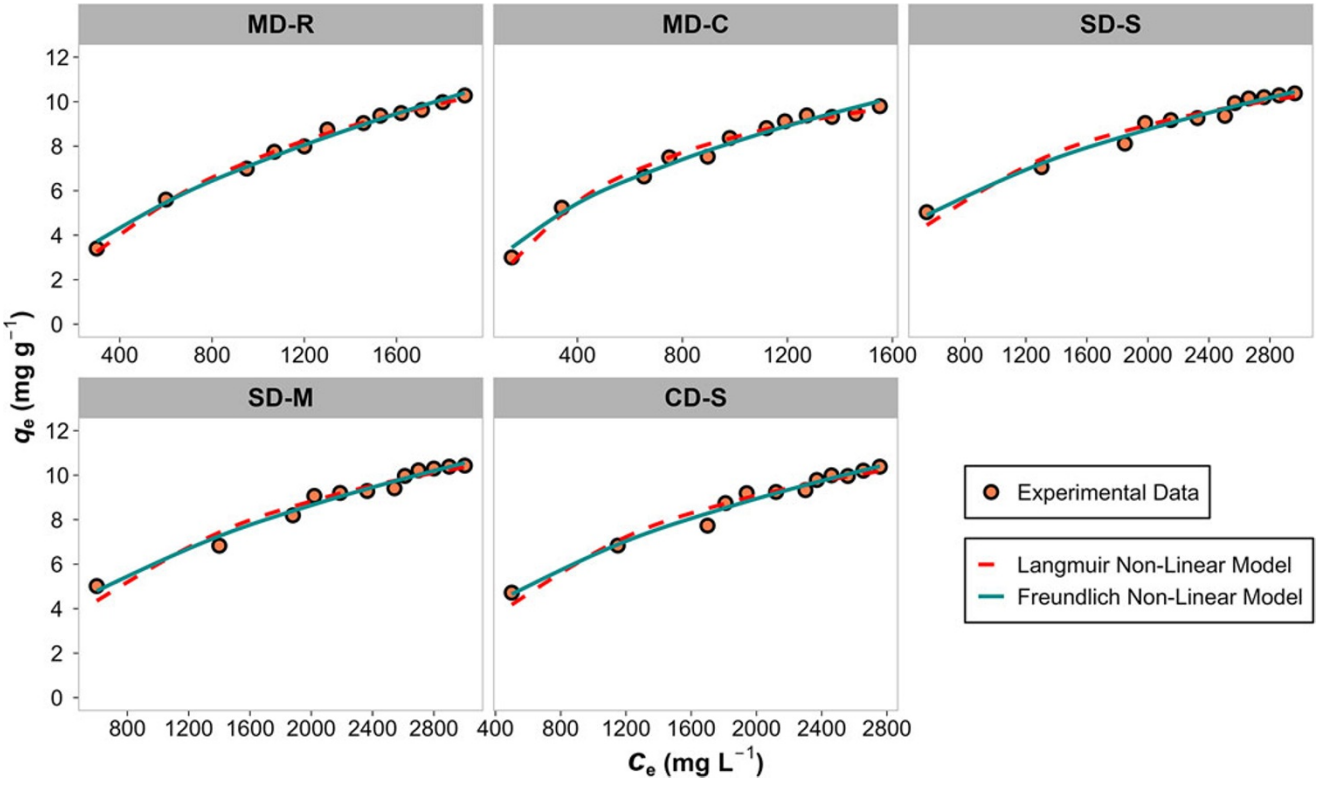

Figure 4. Amount of NH_4^+ adsorbed at equilibrium (q_e) *vs* equilibrium concentration (C_e) plot for the different digestates after a contact time of 24 h.

reinforcing the suitability of the Freundlich model to describe the system. Additionally, the *n* values (commonly used to assess the favourability of adsorption) ranged between 2.04 and 2.28, indicating that the process was favourable in all cases (Wang & Guo, 2020a). Although the differences in *n* values between digestates were not particularly pronounced, those derived from municipal solid waste (MD) exhibited the highest values, particularly for MD-C, suggesting a more favourable adsorption environment in this matrix. The Freundlich constant K_F, which reflects the adsorption capacity, was also higher for MD-derived digestates, confirming their better performance. Moreover, the separation factor (R_L) and Gibbs free energy change ($\Delta G°$) further support this conclusion. The R_L values ranged between 0.2 and 0.8 across all systems (Fig. 5), indicating favourable adsorption (Ivanova *et al.*, 2010). However, as the NH_4^+ concentration decreased (corresponding to near saturation of the zeolitic tuff), R_L increased and approached 1, suggesting a gradual decline in adsorption favourability under these conditions. In terms of thermodynamic behaviour, $\Delta G°$ values

Table 5. Parameters calculated according to the Freundlich (Equation 3) and Langmuir isotherms (Equation 4) at 298.15 K (25°C).

Digestate		Freundlich					Langmuir				
	T (K)	R^2	p-value	K_F (mg g^{-1} (L g^{-1})$^{1/n}$)	n	AIC	R^2	p-value	q_{max} (mg g^{-1})	K_L (L g^{-1})	AIC
MD-R	298.15	0.99	6.84E−12	7.27	2.20	−2.2	0.99	1.12E−12	13.93	1.09	−6.3
MD-C	298.15	0.98	3.32E−10	8.20	2.28	7.2	0.98	2.16E−10	13.24	1.74	6.6
SD-S	298.15	0.98	3.13E−10	6.41	2.11	0.9	0.96	2.20E−08	14.51	0.804	11.8
SD-M	298.15	0.98	1.08E−09	6.16	2.04	4.7	0.96	2.85E−08	15.80	0.634	13.2
CD-S	298.15	0.98	6.56E−10	6.45	2.12	3.8	0.96	1.45E−08	14.93	0.777	11.8

Table 6. Gibbs free energy ($\Delta G°$; Equation 6) and the thermodynamic equilibrium constant (K_e) values determined at 298.15 K (25°C).

Digestate	K_e	$\Delta G°$ (J mol^{-1})
MD-R	11.4	6028
MD-C	18.0	7163
SD-S	9.0	5435
SD-M	8.3	5324
CD-S	9.2	5509

(Table 6) were consistently negative, confirming the spontaneous nature of NH_4^+ adsorption on the zeolitic tuff. The most negative $\Delta G°$ values were observed for MD-C and MD-R, again pointing to the improved performance of MD-derived digestates. These results are in line with other studies using similar materials and experimental conditions (Galamini *et al.*, 2020). Taken together, the combination of kinetic, isotherm and thermodynamic data indicates that NH_4^+ adsorption onto the zeolitic tuff is a spontaneous, favourable and surface-heterogeneous process that is particularly efficient in matrices derived from municipal organic waste.

Effects of digestate composition and pre-treatment methods

One of the key elements influencing the efficiency of NH_4^+ adsorption onto the zeolitic tuff is the physical and chemical composition of the digestates, particularly their TS content and cation concentrations. A high TS content in the digestates can hinder adsorption by promoting pore blockage or competition for adsorption sites due to the presence of suspended organic and inorganic matter (Taddeo *et al.*, 2017; Eberle *et al.*, 2022). A similar pattern was observed in this study (Fig. 6a): the digestate derived from MD-C, which exhibited the lowest TS content, showed the highest NH_4^+ removal, whereas the cattle-derived digestate CD-S, characterized by the highest TS concentration, resulted in the lowest NH_4^+ reduction. These findings are consistent with observations by Eberle *et al.* (2022), who also reported that dissolved organic carbon (DOC) may interfere with NH_4^+ adsorption due to competitive occupation of active sites. Although DOC was not measured in this study, it is expected to be partly correlated with TS, especially in clarified digestate samples. However, the relationship is strongly influenced by the solid–liquid partitioning and specific organic matter composition.

In addition to TS, the chemical composition of the digestate (especially the concentration of monovalent cations) plays a crucial role. Ions such as K^+ and Na^+, due to their similar size and charge to NH_4^+, can strongly compete for adsorption sites in zeolites – often more than divalent cations such as Mg^{2+} and Ca^{2+} (Farkaš *et al.*, 2005; Huang *et al.*, 2015; Ferretti *et al.*, 2020). Potassium in particular has been identified as such a key competitor (Kong *et al.*, 2016). When the K^+ concentrations (Table 1) are compared across the digestates, an inverse relationship between initial K^+ levels and NH_4^+-N removal efficiencies is observed for the MD and swine digestates (Fig. 6b), with lower K^+ (MD-R, MD-C) corresponding to higher NH_4^+ removal and higher K^+ (SD-S, SD-M) corresponding to lower removal, in agreement with Guo *et al.* (2008). Interestingly, the cattle digestate (CD-S, dashed line in Fig. 6b) does not follow this trend: despite its greater K^+ content, it exhibits greater NH_4^+ removal than the swine digestates. This unexpected behaviour may be influenced by other cations, such

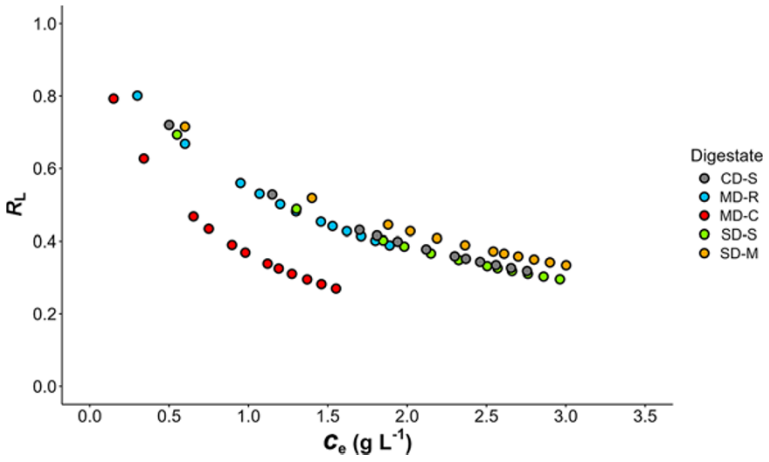

Figure 5. Separation factor (R_L) *vs* equilibrium concentration (C_e) for the different digestates.

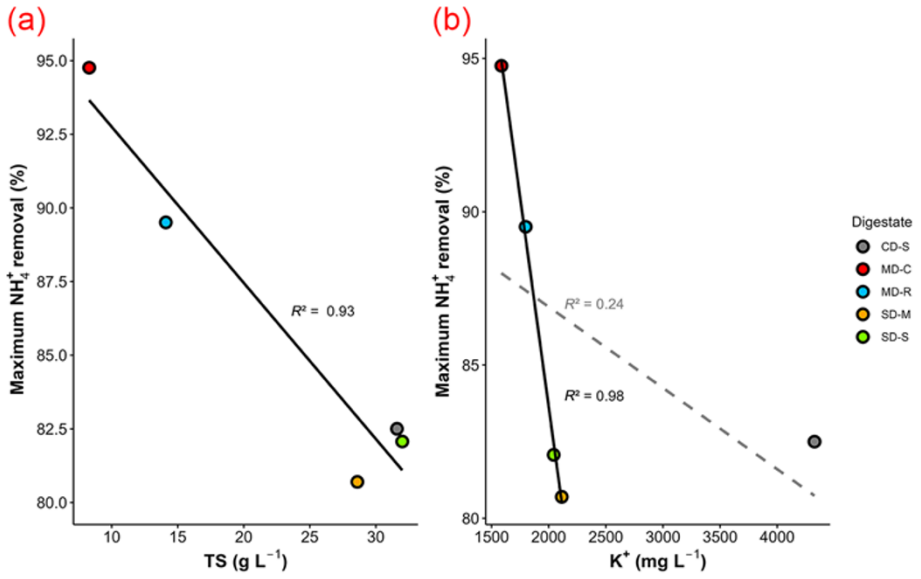

Figure 6. Linear regression between the maximum NH_4^+ removal efficiency (R_E) and (a) TS content and (b) potassium (K^+) content for the different digestates. The equilibrium NH_4^+ R_E was used as the response variable. In (b), the dashed grey regression line includes all five digestate types, whereas the solid black line excludes CD-S, which exhibits a distinct behaviour.

as the lower Na^+ and Ca^{2+} concentrations in CD-S, which could modulate NH_4^+ adsorption.

Our findings are at odds with the classical expectation that a greater initial NH_4^+ concentration increases adsorption by increasing the mass transfer driving force (Demir *et al.*, 2002). In this study, however, greater NH_4^+ reduction occurred in matrices with lower initial NH_4^+ concentrations – an effect also noted by Kotoulas *et al.* (2019) and Taddeo *et al.* (2017). This deviation suggests that, in complex matrices such as digestates, other limiting factors such as TS content and ion competition may outweigh the driving force effect. Digestates with more favourable physical and chemical profiles, such as MD-derived ones, consistently demonstrated superior performance in terms of NH_4^+ reduction, despite their lower starting concentrations.

To mitigate the negative impact of solids and ionic competition, various pre-treatments could be applied, such as clarification, microfiltration and screw compression (Chini *et al.*, 2021; Nowak & Czekała, 2024). Pre-treated samples displayed lower $1/n$ values, more negative $\Delta G°$ values (Table 6) and R_L values closer to zero (Fig. 5), suggesting the increased affinity, spontaneity and favourability of the NH_4^+ adsorption process. These outcomes were also reflected in faster equilibrium times and greater overall NH_4^+ reductions.

Such results align with similar previous studies (Proskynitopoulou *et al.*, 2024) that affirm that removing solids through centrifugation or filtration can improve accessibility to zeolite-exchange sites, thus improving performance. The greatest difference in NH_4^+ reduction (Fig. 3a) was observed between MD-R and MD-C, suggesting that performing a centrifugation step prior to NH_4^+ adsorption is the most effective strategy for improving NH_4^+ removal from a digestate. In contrast, the microfiltration step also increased NH_4^+ adsorption by the zeolitic tuff, but this improvement was less pronounced. From an applied perspective, integrating pre-treatment strategies into the treatment chain could significantly improve the efficiency of zeolite-based NH_4^+ recycling systems, particularly when dealing with livestock-derived effluents or complex digestates.

Effects of zeolite type and amount: comparative evaluation

To assess the role of zeolite mineralogy in NH_4^+ recovery from digestates, the performance of the chabazite-rich tuff tested in this study was directly compared with the data from Alberghini *et al.* (2025), who employed a zeolitic tuff composed of both phillipsite and chabazite. The comparison was carried out under identical

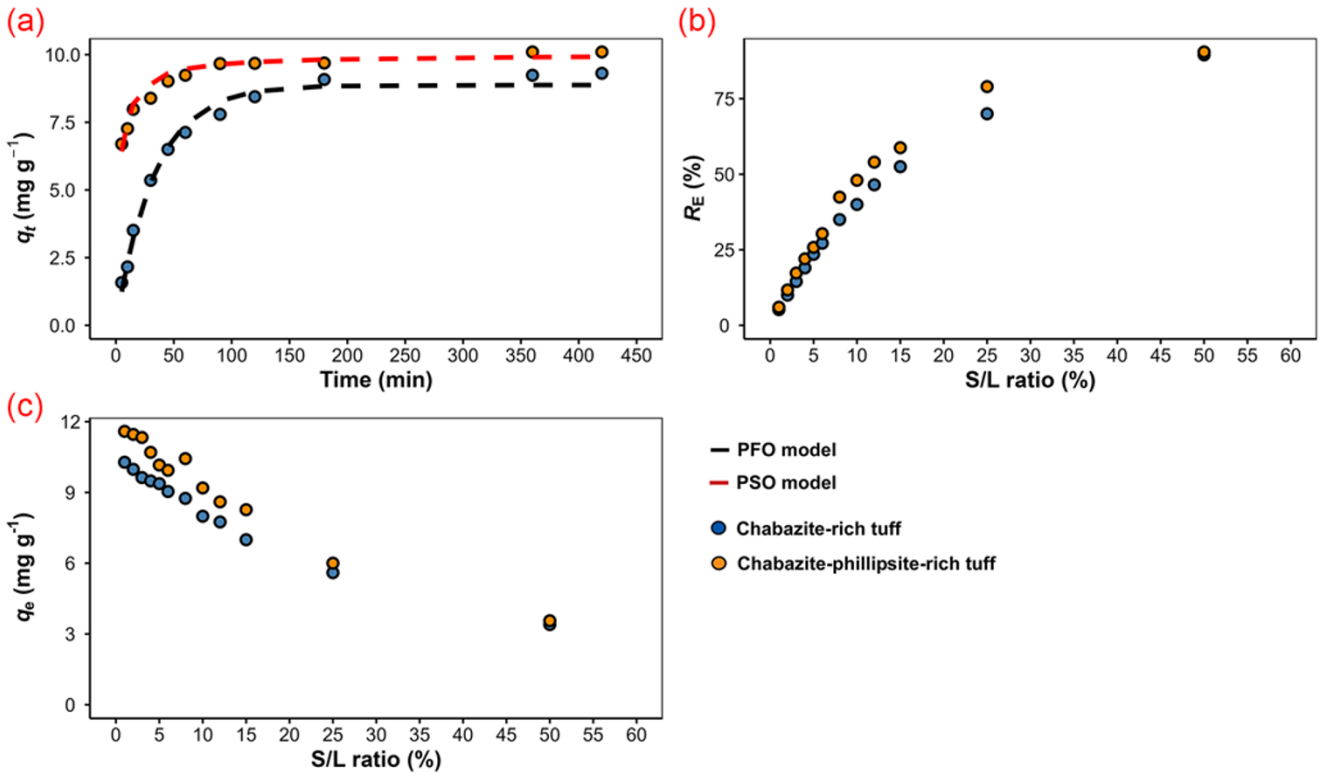

Figure 7. Comparison between chabazite-rich and phillipsite–chabazite-rich tuffs in terms of (a) adsorption kinetics (q_t *vs* time), (b) NH_4^+ removal efficiency (R_E) as a function of S/L ratio and (c) amount of NH_4^+ adsorbed at equilibrium (q_e) as a function of S/L ratio. Results refer to the MD-R digestate, which was selected as a representative case due to the more pronounced differences observed between the two materials in terms of adsorption kinetics, NH_4^+ removal and capacity. Data for the chabazite–phillipsite-rich tuff are from Alberghini *et al.* (2025).

experimental conditions, using the same digestates (MD, swine and cattle digestates), experimental setup and data analysis methods.

The kinetic analysis revealed substantial differences in the NH_4^+ uptake behaviour between the two zeolitic tuffs, attributable to their distinct mineralogical composition and cation-exchange properties. The NH_4^+ removal kinetics were well described by the PFO model, where the rate is initially fast and slows down as equilibrium is approached. This behaviour, which is common in zeolitic adsorbents, reflects processes often governed by surface diffusion or external mass transfer. In contrast, the chabazite–phillipsite-rich tuff showed a better fit with the PSO model, implying a more complex process probably involving multilayer adsorption or chemisorption interactions, consistent with a more heterogeneous surface environment (Halim *et al.*, 2010; Shaban *et al.*, 2017).

The faster initial uptake rates observed for the chabazite-rich tuff are indicative of a strong driving force for ion exchange in the early phase, followed by rapid attainment of equilibrium (typically within 90–180 min). In contrast, the chabazite–phillipsite-rich tuff generally reached equilibrium within 45–120 min, probably due to the enhanced surface heterogeneity and microporosity conferred by the dual-zeolite phases and greater glass content. This difference in equilibrium time was particularly marked in the MD-R digestate, where the chabazite–phillipsite-rich tuff achieved equilibrium significantly faster than the chabazite-rich tuff (Fig. 7a). Moreover, in the same digestate, the difference between the two materials was also more evident in terms of R_E and q_e (Fig. 7b,c). Nonetheless, the differences observed for these two parameters were not pronounced, highlighting that the chabazite-rich tuff still performed very well and represents a highly suitable option for NH_4^+ recovery from digestates.

The application of the ID model further supported a multi-step adsorption process in both materials, characterized by an initial external surface sorption phase, a gradual ID stage and final equilibration (Zhou *et al.*, 2024). However, the deviations from linearity and the absence of plot intercepts through the origin indicate that, although ID contributes to NH_4^+ uptake, it is not the sole rate-controlling process. This is especially evident for the chabazite–phillipsite-rich tuff, for which diffusion into micropores may be more influential due to the presence of a more heterogeneous pore structure.

These kinetic insights align well with the equilibrium results obtained from Freundlich isotherm modelling, which further emphasized differences in sorption performance between the two rocks. The chabazite-rich tuff generally exhibited lower K_F values across all digestates, except for MD-C, where the values were similar (8.20 *vs* 8.47 mg g^{-1}(L g^{-1})$^{1/n}$). The highest K_F value observed for the chabazite–phillipsite-rich tuff was 9.06 (MD-R), compared to 8.20 for the chabazite-rich tuff, confirming a slightly reduced adsorption capacity when phillipsite is absent. Despite these differences, the Freundlich *n* values remained within a comparable range (1.78–2.59), indicating similar adsorption intensities and surface heterogeneities between the two materials (Haghseresht & Lu, 1998).

Thermodynamic parameters further enriched the comparative analysis. In both materials, $\Delta G°$ values ranged from approximately −5000 to −7200 J mol^{-1}, confirming the spontaneous nature of the process and its predominantly physical character

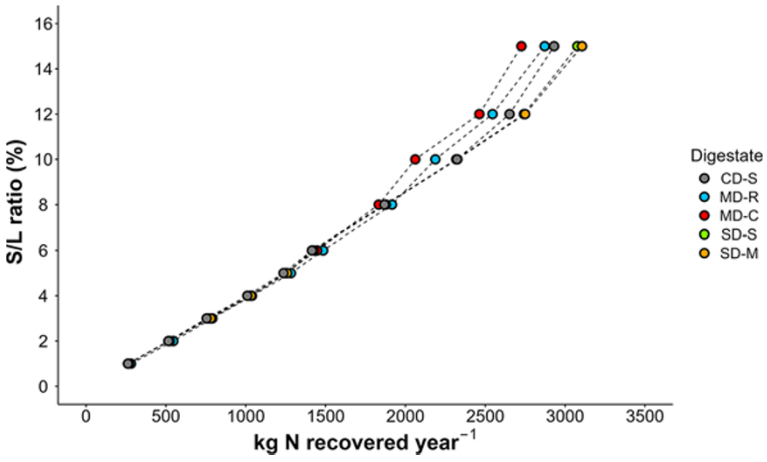

Figure 8. Values of kg N recovered year^{-1} as a function of the S/L ratio of the zeolitic tuff used during the experiment.

(Jha & Hayashi, 2009). Interestingly, the chabazite-rich tuff exhibited slightly more negative $\Delta G°$ values than the phillipsite–chabazite-rich tuff for certain digestates (e.g. MD-C: −7163 *vs* −7024 J mol^{-1}; CD-S: −5509 *vs* −5075 J mol^{-1}), suggesting a marginally more favourable energetic profile for NH_4^+ sorption on pure chabazite.

These results can be rationalized by considering the distinct physicochemical properties of the two tuffs. The chabazite–phillipsite-rich tuff had a slightly higher CEC (233 cmol kg^{-1}) compared to the chabazite-rich tuff (217 cmol kg^{-1}), which is consistent with the greater sorption capacity observed. Moreover, the mineralogical composition differed markedly: the former contained ∼20% chabazite, 10% phillipsite and 44% volcanic glass, whereas the latter consisted predominantly of chabazite (68.5%), with only 1.8% phillipsite and 11.0% volcanic glass. The greater glass content and dual-zeolite phase in the previous material probably increased surface heterogeneity and microporosity, promoting multilayer interactions and diffusion-limited uptake. Moreover, the presence of nanocrystalline domains within the amorphous phase (potentially of a zeolitic nature; Leggo *et al.*, 2001; Holder & Schaak, 2019) could further contribute to NH_4^+ adsorption, thereby explaining the greater sorption capacity observed for this zeolitic tuff. Conversely, the chabazite-rich tuff, with its simpler phase composition and greater abundance of exchange sites per unit mass, favoured faster, surface-dominated ion exchange, but with a slightly reduced capacity.

This comparative evaluation underscores how mineralogy and CEC critically shape both the kinetics and thermodynamics of NH_4^+ adsorption. Although phillipsite improves overall sorption capacity and introduces more complex uptake mechanisms, chabazite alone provides an energetically favourable and kinetically efficient pathway for NH_4^+ removal from digestates. These findings are pivotal for guiding the selection and optimization of natural zeolitic materials in nutrient recovery applications.

Scalability assessment of nitrogen recovery from anaerobic digestate

Using the same calculation method described in our previous work (Alberghini *et al.*, 2025), the potential nitrogen recovery (see earlier) was estimated for each digestate matrix under realistic operational conditions at the farm scale. Assuming an average daily production of 10 m^3 of digestate per plant with continuous operation throughout the year, the annual nitrogen recovery was calculated as a function of S/L ratio, up to a maximum of 15%, a value considered feasible for practical application at the farm level.

Figure 8 shows that the amount of nitrogen potentially recoverable on an annual basis varies significantly depending on the digestate type and S/L ratio. As expected, livestock-derived digestates (particularly SD-S and SD-M) showed greater recovery values due to their greater NH_4^+ concentrations and faster adsorption kinetics, which enable a higher number of treatment cycles per day. At an S/L ratio of 15%, the maximum nitrogen recovery reached values exceeding 3000 kg N year^{-1} per plant for these matrices.

Conversely, although municipal solid waste-derived digestates (MD-R and MD-C) allowed for a lower absolute nitrogen recovery (due to lower initial NH_4^+-N concentrations and slower kinetics), they showed higher percentages of NH_4^+ reduction during treatment, as discussed in previous sections. These matrices may therefore be more suitable in contexts in which the treatment objective is primarily the reduction of nitrogen load rather than its recovery.

Compared to the study with a chabazite–phillipsite-rich tuff (Alberghini *et al.*, 2025), the chabazite-rich tuff of the present study provided comparable or slightly lower nitrogen recovery yields across most conditions. For a consistent comparison, the previous data were recalculated to account for the contact time needed to reach equilibrium, as well as the additional time required for loading and unloading the pilot-scale prototype. Despite slightly lower total yields in some cases, the chabazite-rich tuff consistently achieved higher annual nitrogen recovery, particularly in more complex matrices such as swine and cattle digestates. This improved performance is probably related to its robustness under high organic loads and varying ionic strengths, suggesting that chabazite may be more adaptable under real operational conditions. A detailed comparison of these parameters is provided in Table S1.

Overall, even at relatively low S/L ratios, the annual nitrogen recovery potential remains relevant across all digestate types. This reinforces the potential of NH_4^+-enriched zeolitic tuff to be reused as a slow-release fertilizer in agriculture, partially replacing synthetic fertilizers such as urea. This substitution would align with the sustainability goals promoted by the European Green Deal by reducing both the environmental impacts and the energy demands associated with synthetic nitrogen fertilizer production (Di Giuseppe *et al.*, 2016; Ali *et al.*, 2017; Eroglu *et al.*, 2017; Ghasemi *et al.*, 2018; Mpanga *et al.*, 2020; Cataldo *et al.*, 2021; Jarosz *et al.*, 2022; Galamini *et al.*, 2023; Ferretti *et al.*, 2024).

To validate the theoretical framework under practical conditions, a preliminary field application was performed in a test plant belonging to the project 'STRUVITE' (funded through the PR-FESR Emilia-Romagna 2021–2027 programme). The prototype machine could treat a maximum of 2 m^3 per cycle. The tests were performed in May 2025 using microfiltered swine digestate (SD-M) at a zeolite S/L ratio of 3% (dry basis). The treatment was conducted in a discontinuous batch mode with three cycles per day, each processing 2 m^3 of digestate (total 6 m^3 day^{-1}). Each cycle included ∼1.5 h of effective contact time between the zeolite and the digestate, plus an additional ∼20 min before and after the cycle for prototype loading and unloading. Each batch resulted in an average NH_4^+ removal of ∼10% of the initial concentration, corresponding to a zeolite loading of ∼11 g NH_4^+-N per kg of dry zeolite. This value is consistent with the results obtained in laboratory tests, confirming the reliability of the proposed batch setup and the practical relevance of the findings. During the treatment, the pH of the digestate increased slightly, from an average of 7.6 to 7.8 before and after contact with the zeolite, indicating a mild alkalinization of the system, in line with previous studies reporting similar effects of zeolite application on wastewater and digestate treatment (Ferretti *et al.*, 2020; Myrzalieva *et al.*, 2021; Teymouri *et al.*, 2024). Based on this configuration, the estimated annual nitrogen recovery was ∼715 kg N $year^{-1}$. Future scale-up is planned in terms of using a continuous-flow system, which is expected to significantly increase the daily throughput and improve the overall nitrogen recovery efficiency.

Conclusions

This study highlights the potential of a chabazite-rich tuff as a sustainable and efficient adsorbent for NH_4^+ recovery from various anaerobic digestates, with direct implications for farm-scale applications. The results confirm that the chabazite-rich zeolitic tuff is a promising material for ammonium recovery from various digestates. Adsorption followed a multilayer and heterogeneous process (Freundlich isotherm), with its kinetics best described by the PFO model. Digestate composition (especially K^+ levels and TS content) significantly influenced NH_4^+ uptake. Livestock-derived digestates ensured the greatest recovery, while solid–liquid separation (particularly centrifugation) improved performance by increasing site accessibility. A preliminary field-scale trial with microfiltered swine digestate demonstrated process feasibility, with a potential recovery of up to ∼715 kg N $year^{-1}$ per plant, supporting its integration into circular nutrient management strategies. Compared to previous findings involving a zeolitic tuff containing both phillipsite and chabazite, the chabazite-rich tuff used in this study showed distinct adsorption behaviour under the same operating conditions. These differences, related to mineralogical composition and CEC, will be the basis for future comparative studies aiming to optimize zeolite selection based on kinetic performance, adsorption capacity and process simplicity. It is considered that by enhancing our understanding of the process through exploring the behaviour of other commercially available zeolite tuffs (e.g. clinoptilolite-rich tuffs), it will be possible to increase the applicability of this technology under diverse operational scenarios. Overall, these findings highlight the potential of zeolite-based systems for circular nitrogen management in agriculture, enabling the recovery of valuable nutrients from organic wastes while reducing reliance on synthetic fertilizers, in line with European Green Deal objectives and supporting more resilient and sustainable food systems. The NH_4^+-saturated tuff produced through this process can be applied directly as a slow-release soil amendment, and although the chabazite-rich tuff studied here showed comparable nitrogen recovery to the chabazite–phillipsite-rich tuff, it stands out for its consistently robust and adaptable NH_4^+ removal performance, even in complex matrices.

Supplementary material. The supplementary material for this article can be found at https://doi.org/10.1180/clm.2026.10025.

Author contributions. Conceptualization: Matteo Alberghini, Giacomo Ferretti; Methodology: Matteo Alberghini, Giacomo Ferretti; Investigation: Matteo Alberghini, Giacomo Ferretti; Writing – Original draft: Matteo Alberghini; Writing – Review and editing: Matteo Alberghini, Giacomo Ferretti; Supervision: Matteo Alberghini, Giacomo Ferretti; Formal analysis: Matteo Alberghini, Cristina Botezatu; Data curation: Matteo Alberghini, Giacomo Ferretti; Project administration: Giacomo Ferretti, Barbara Faccini; Data analysis: Matteo Alberghini, Giacomo Ferretti; Validation: Giacomo Ferretti; Resources: Giacomo Ferretti, Barbara Faccini. All authors have read and agreed to the published version of the manuscript.

Acknowledgements. We acknowledge the support of CRPA (Emilia-Romagna) and WAM Group for their technical assistance. We also extend our gratitude to Biorg and Colombaro for supplying the various digestate samples utilized in this research. We further thank Verdi S.p.A. for providing the zeolitic tuff used in this study. We gratefully acknowledge Renzo Tassinari for performing the ICP-MS analyses.

Financial support. This work was supported by the project 'STRUVITE – Trattamento dei digestati per ridurre le emissioni e recuperare un fertilizzante, la Struvite', funded through the PR-FESR Emilia-Romagna 2021–2027 programme.

Competing interests. The authors declare none.

Data availability. All relevant data for this study are available in the manuscript and accompanying Supplementary Material.

References

Alberghini M., Ferretti G., Galamini G., Botezatu C. & Faccini B. (2025) Selective ammonium recovery from livestock and organic solid waste digestates using zeolite tuff: efficiency and farm-scale prospects. *Recycling*, **10**, 137.

Ali S., Nakhli A. & Delkash M. (2017) Application of zeolites for sustainable agriculture: a review on water and nutrient retention. *Water, Air, & Soil Pollution*, **228**, 464.

Banik C., Bakshi S., Andersen D.S., Laird D.A., Smith R.G. & Brown R.C. (2023) The role of biochar and zeolite in enhancing nitrogen and phosphorus recovery: a sustainable manure management technology. *Chemical Engineering Journal*, **456**, 141003.

Cataldo E., Salvi L., Paoli F., Fucile M., Masciandaro G., Manzi D. *et al.* (2021) Application of zeolites in agriculture and other potential uses: a review. *Agronomy*, **11**, 1547.

Cheary R.W., Coelho A.A. & Cline J.P. (2004) Fundamental parameters line profile fitting in laboratory diffractometers. *Journal of Research of the National Institute of Standards and Technology*, **109**, 1–25.

Chen H.F., Lin Y.J., Chen B.H., Yoshiyuki I., Liou S.Y.H. & Huang R.T. (2018) A further investigation of NH_4^+ removal mechanisms by using natural and synthetic zeolites in different concentrations and temperatures. *Minerals*, **8**, 499.

Cheng Z. & Ding W. (2015) Ammonium removal from water by natural and modified zeolite: kinetic, equilibrium, and thermodynamic studies. *Desalination and Water Treatment*, **55**, 978–985.

Chini A., Hollas C.E., Bolsan A.C., Antes F.G., Treichel H. & Kunz A. (2021) Treatment of digestate from swine sludge continuous stirred tank reactor to reduce total carbon and total solids content. *Environment, Development and Sustainability*, **23**, 12326–12341.

Coombs D.S., Alberti A., Armbruster T., Artioli G., Colella C., Galli E. *et al.* (1998) Recommended nomenclature for zeolite minerals: report of the subcommittee on zeolites of the international mineralogical association, commission on new minerals and mineral names. *Mineralogical Magazine*, **62**, 533–571.

Dal Verme M., Lipari D., Lucido G., Maio V., Surace V. & Liberatore P. (2021) *Statistical Report 2021: Renewable Energy Sources in Italy*. GSE – Gestore dei Servizi Energetici, Rome, Italy.

Damodara A.K. & Parameswaran P. (2021) Ammonia adsorption and recovery from swine wastewater permeate using naturally occurring clinoptilolite. *Journal of Water Process Engineering*, **43**, 102234.

Demir A., Günay A. & Debik E. (2002) Ammonium removal from aqueous solution by ion-exchange using packed bed natural zeolite. *Water SA*, **28**, 329–335.

Deocaris C.C. & De Osio L.P. (2020) Fitting Henry's adsorption isotherm model in *R* using *PUPAIM* package. *Asia Pacific Journal of Research*, **1**, 47–51.

Detho A., Memon A.A., Memon A.H., Almohana A.I., Daud Z. & Rosli M.A. (2023) Sorption kinetics, isotherm studies and mechanism of removal of organic and inorganic by adsorption onto renewable biomineral. *Water, Air, & Soil Pollution*, **234**, 1–11.

Di Giuseppe D., Ferretti G., Faccini B., Blasi E., Passeri N., Bianchini G. & Coltorti M. (2016) Is it possible to cultivate corn in a sustainable way using a quarry waste? *Periodico di Mineralogia*, **85**, 179–183.

Dyer A. & Zubair M. (1998) Ion-exchange in chabazite. *Microporous and Mesoporous Materials*, **22**, 135–150.

Eberle S., Börnick H. & Stolte S. (2022) Granular natural zeolites: cost-effective adsorbents for the removal of ammonium from drinking water. *Water*, **14**, 939.

Eroglu N., Emekci M. & Athanassiou C.G. (2017) Applications of natural zeolites on agriculture and food production. *Journal of the Science of Food and Agriculture*, **97**, 3487–3499.

European Biogas Association (2022) *Exploring Digestate's Contribution to Healthy Soils*. European Biogas Association, Brussels, Belgium, 39 pp.

European Commission (2020) Farm to Fork Strategy. DG SANTE – Unit Food Information, Composition and Food Waste. Available at https://food.ec.europa.eu/horizontal-topics/farm-fork-strategy_en.

European Union (1998) Council Directive 98/83/EC of 3 November 1998 on the quality of water intended for human consumption. *Official Journal of the European Communities*, **L330**, 32–54.

Faccini B., Di Giuseppe D., Malferrari D., Coltorti M., Abbondanzi F., Campisi T. *et al.* (2015) Ammonium-exchanged zeolitite preparation for agricultural uses: from laboratory tests to large-scale application in ZeoLIFE project prototype. *Periodico di Mineralogia*, **84**, 303–321.

FAO (2009) How to feed the world in 2050. Presented at *Expert Meeting on How to Feed the World in 2050*, Rome, Italy, 24–26 June.

Farkaš A., Rožić M. & Barbarić-Mikočević Ž. (2005) Ammonium exchange in leakage waters of waste dumps using natural zeolite from the Krapina region, Croatia. *Journal of Hazardous Materials*, **117**, 25–33.

Ferretti G., Galamini G., Medoro V., Coltorti M., Di Giuseppe D. & Faccini B. (2020) Impact of sequential treatments with natural and Na-exchanged chabazite zeolite-rich tuff on pig-slurry chemical composition. *Water*, **12**, 310.

Ferretti G., Rosinger C., Diaz-Pines E., Faccini B., Coltorti M. & Keiblinger K.M. (2024) Soil quality increases with long-term chabazite-zeolite tuff amendments in arable and perennial cropping systems. *Journal of Environmental Management*, **354**, 120303.

Freundlich H.M.F. (1906) Over the adsorption in solution. *Journal of Physical Chemistry*, **57**, 1100–1107.

Fu H., Li Y., Yu Z., Shen J., Li J., Zhang M. *et al.* (2020) Ammonium removal using a calcined natural zeolite modified with sodium nitrate. *Journal of Hazardous Materials*, **393**, 122481.

Galamini G., Ferretti G., Medoro V., Tescaro N. & Faccini B. (2020) Isotherms, kinetics, and thermodynamics of NH_4^+ adsorption in raw liquid manure by using natural chabazite zeolite-rich tuff. *Water*, **12**, 2944.

Galamini G., Ferretti G., Rosinger C., Huber S., Medoro V., Mentler A. *et al.* (2023) Recycling nitrogen from liquid digestate *via* novel reactive struvite and zeolite minerals to mitigate agricultural pollution. *Chemosphere*, **317**, 137881.

Galamini G., Ferretti G., Medoro V., Eftekhari N., Favero M., Faccini B. & Coltorti M. (2024) Applying natural and K-enriched zeolite before struvite precipitation improved the recovery of NH_4^+ from liquid digestate and the reagent use efficiency. *International Journal of Environmental Research*, **18**, 1–13.

Galamini G., Ferretti G., Rosinger C., Huber S., Mentler A., Pines E.D. *et al.* (2025) Potential for agricultural recycling of struvite and zeolites to improve soil microbial physiology and mitigate CO_2 emissions. *Geoderma*, **453**, 117149.

Ghasemi Z., Sourinejad I., Kazemian H. & Rohani S. (2018) Application of zeolites in aquaculture industry: a review. *Reviews in Aquaculture*, **10**, 75–95.

Guo X., Zeng L., Li X. & Park H.S. (2008) Ammonium and potassium removal for anaerobically digested wastewater using natural clinoptilolite followed by membrane pretreatment. *Journal of Hazardous Materials*, **151**, 125–133.

Haghseresht F. & Lu G.Q. (1998) Adsorption characteristics of phenolic compounds onto coal-reject-derived adsorbents. *Energy & Fuels*, **12**, 1100–1107.

Halim A.A., Aziz H.A., Johari M.A.M. & Ariffin K.S. (2010) Comparison study of ammonia and COD adsorption on zeolite, activated carbon and composite materials in landfill leachate treatment. *Desalination*, **262**, 31–35.

Ho Y.S. & McKay G. (1998) A comparison of chemisorption kinetic models applied to pollutant removal on various sorbents. *Process Safety and Environmental Protection*, **76**, 332–340.

Holder C.F. & Schaak R.E. (2019) Tutorial on powder X-ray diffraction for characterizing nanoscale materials. *ACS Nano*, **13**, 7359–7365.

Hooda P.S., Edwards A.C., Anderson H.A. & Miller A. (2000) A review of water quality concerns in livestock farming areas. *Science of the Total Environment*, **250**, 143–167.

Hou J., Huang L., Yang Z., Zhao Y. & Deng C. (2016) Adsorption of ammonium on biochar prepared from giant reed. *Environmental Science and Pollution Research*, **23**, 19107–19115.

Huang H., Xiao X., Yan B. & Yang L. (2010) Ammonium removal from aqueous solutions by using natural Chinese (Chende) zeolite as adsorbent. *Journal of Hazardous Materials*, **175**, 247–252.

Huang H., Yang L., Xue Q., Liu J., Hou L. & Ding L. (2015) Removal of ammonium from swine wastewater by zeolite combined with chlorination for regeneration. *Journal of Environmental Management*, **160**, 333–341.

Huang J., Kankanamge N.R., Chow C., Welsh D.T., Li T. & Teasdale P.R. (2017) Removing ammonium from water and wastewater using cost-effective adsorbents: a review. *Journal of Environmental Sciences*, **63**, 174–197.

Huygens D., Orveillon G., Lugato E. & Tavazzi S. (2020) *Technical Proposals for the Safe Use of Processed Manure Above the Threshold Established for Nitrate Vulnerable Zones by the Nitrates Directive (91/676/EEC)*. Publications Office of the European Union, Luxembourg, 163 pp.

Ivanova E., Karsheva M. & Koumanova B. (2010) Adsorption of ammonium ions onto natural zeolite. *Journal of the University of Chemical Technology and Metallurgy*, **45**, 295–302.

Jarosz R., Szerement J., Gondek K. & Mierzwa-Hersztek M. (2022) The use of zeolites as an addition to fertilisers – a review. *Catena*, **213**, 106125.

Jha V.K. & Hayashi S. (2009) Modification on natural clinoptilolite zeolite for its NH_4^+ retention capacity. *Journal of Hazardous Materials*, **169**, 29–35.

Karaçetin G., Sivrikaya S. & Imamoğlu M. (2014) Adsorption of methylene blue from aqueous solutions by activated carbon prepared from hazelnut husk using zinc chloride. *Journal of Analytical and Applied Pyrolysis*, **110**, 270–276.

Khan A.A. & Singh R.P. (1987) Adsorption thermodynamics of carbofuran on Sn(IV) arsenosilicate in H^+, Na^+ and Ca^{2+} forms. *Colloids and Surfaces*, **24**, 33–42.

Kong M., Liu Z., Vogt T. & Lee Y. (2016) Chabazite structures with Li^+, Na^+, Ag^+, K^+, NH_4^+, Rb^+ and Cs^+ as extra-framework cations. *Microporous and Mesoporous Materials*, **221**, 253–263.

Kotoulas A., Agathou D., Triantaphyllidou I.E., Tatoulis T.I., Akratos C.S., Tekerlekopoulou A.G. & Vayenas D.V. (2019) Zeolite as a potential medium for ammonium recovery and second cheese whey treatment. *Water*, **11**, 136.

Kovačić Đ., Lončarić Z., Jović J., Samac D., Popović B. & Tišma M. (2022) Digestate management and processing practices: a review. *Applied Sciences*, **12**, 9216.

Lagergren S. (1898) About the theory of so-called adsorption of soluble substances. *Kungliga Svenska Vetenskapsakademiens Handlingar*, **24**, 1–39.

Leggo P.J., Cochemé J.J., Demant A. & Lee W.T. (2001) The role of argillic alteration in the zeolitization of volcanic glass. *Mineralogical Magazine*, **65**, 653–663.

Lin L., Lei Z., Wang L., Liu X., Zhang Y., Wan C. *et al.* (2013) Adsorption mechanisms of high levels of ammonium onto natural and NaCl-modified zeolites. *Separation and Purification Technology*, **103**, 15–20.

Liu Y., Zhang P., Liu A., Liu Z., Liu X., Yang L. & Yang Y. (2022) Adsorption mechanism of high-concentration ammonium by Chinese natural zeolite with experimental optimization and theoretical computation. *Water*, **14**, 2413.

Magalong J.R., DelaCruz J., Bumatay J. & Deocaris C. (2022) *PUPAK*: parameter estimation and plot visualization of adsorption kinetic models. *CRAN Repository*. Available at https://doi.org/10.32614/CRAN.package.PUPAK.

Makádi M., Tomócsik A. & Orosz V. (2012) Digestate: a new nutrient source – review. Pp. 295–310 in: *Biogas* (S. Kumar, editor). InTech, London, UK.

Malferrari D., Laurora A., Brigatti M.F., Coltorti M., Di Giuseppe D., Faccini B. *et al.* (2013) Open-field experimentation of an innovative and integrated zeolitite cycle: project definition and material characterization. *Rendiconti Lincei*, **24**, 141–150.

Martinez J., Dabert P., Barrington S. & Burton C. (2009) Livestock waste treatment systems for environmental quality, food safety, and sustainability. *Bioresource Technology*, **100**, 5527–5536.

Mazloomi F. & Jalali M. (2016) Ammonium removal from aqueous solutions by natural zeolite in the presence of organic acids, cations and anions. *Journal of Environmental Chemical Engineering*, **4**, 1664–1673.

Moussavi G., Talebi S., Farrokhi M. & Sabouti R.M. (2011) The investigation of mechanism, kinetic and isotherm of ammonia and humic acid co-adsorption onto natural zeolite. *Chemical Engineering Journal*, **171**, 1159–1169.

Mpanga I.K., Braun H. & Walworth J. (2020) Zeolite application in crop production: importance to soil nutrient, soil water, soil health, and environmental pollution management. *Soil Systems*, **4**, 1–4.

Muscarella M.S., Laudicina V.A., Cano B., Badalucco L., Conte P. & Mannina G. (2023) Recovering ammonium by treated and untreated zeolitic mixtures: a comprehensive experimental and modelling study. *Microporous and Mesoporous Materials*, **349**, 112434.

Myrzalieva S., Putra Pratama G.N.I. & Khamidulla A. (2021) Wastewater treatment using natural zeolite materials. *Complex Use of Mineral Resources*, **317**, 64–68

Nguyen M.L. & Tanner C.C. (1998) Ammonium removal from wastewaters using natural New Zealand zeolites. *New Zealand Journal of Agricultural Research*, **41**, 427–446.

Nguyen T.D., Nguyen T.M.P., Van H.T., Nguyen V.Q., Nguyen L.H., Nguyen T.D. *et al.* (2022) Adsorption removal of ammonium using Mg/Al layered double hydroxides–zeolite composite. *Environmental Technology & Innovation*, **25**, 102244.

Nhubu T., Mbohwa C. & Muzenda E. (2020) Eutrophication impact potential of solid waste management options in Harare. *Wastes: Solutions, Treatments and Opportunities*, **III**, 360–366.

Nowak M. & Czekała W. (2024) Sustainable use of digestate from biogas plants: separation of raw digestate and liquid fraction processing. *Sustainability*, **16**, 5461.

Pan M., Zhang M., Zou X., Zhao X., Deng T., Chen T. & Huang X. (2019) The investigation into the adsorption removal of ammonium by natural and modified zeolites: kinetics, isotherms, and thermodynamics. *Water SA*, **45**, 648–656.

Pesendorfer S. & Ellersdorfer M. (2021) Kinetics of simultaneous ammonium and phosphate recovery by natural zeolite. *ChemEngineering*, **5**, 68.

Plazinski W., Rudzinski W. & Plazinska A. (2009) Theoretical models of sorption kinetics including a surface reaction mechanism: a review. *Advances in Colloid and Interface Science*, **152**, 2–13.

Policastro G. & Cesaro A. (2023) Composting of organic solid waste of municipal origin: the role of research in enhancing its sustainability. *International Journal of Environmental Research and Public Health*, **20**, 312.

Proskynitopoulou V., Garagounis I., Vourros A., Dimopoulos Toursidis P., Lorentzou S. & Zouboulis A. (2024) Nutrient recovery from digestate: pilot test experiments. *Journal of Environmental Management*, **353**, 120166.

R Core Team (2021) *R*: a language and environment for statistical computing. R Foundation for Statistical Computing, Vienna, Austria. Available at https://www.r-project.org/.

Rossi G., Beni C., Benedetti A., Felici B. & Neri U. (2023) Effect of mineral or OFMSW digestate fertilization on ryegrass and nitrogen leaching. *Agronomy*, **13**, 1316.

Sánchez-Hernández R., Padilla I. & López-Andrés S. (2018) Al-waste-based zeolite adsorbent used for the removal of ammonium from aqueous solutions. *Advances in Materials Science and Engineering*, **2018**, 1256197.

Shaban M., AbuKhadra M.R., Nasief F.M. & Abd El-Salam H.M. (2017) Removal of ammonia from aqueous solutions, ground water, and wastewater using mechanically activated clinoptilolite and synthetic zeolite-A: kinetic and equilibrium studies. *Water, Air, & Soil Pollution*, **228**, 11.

Simonin J.P. (2016) On the comparison of pseudo-first order and pseudo-second order rate laws in the modeling of adsorption kinetics. *Chemical Engineering Journal*, **300**, 254–263.

Susilawati S., Andriayani A., Sihombing Y.A., Saragi I., Masruchin N., Nuryawan A. & Irma M. (2025) Study of ammonium adsorption mechanism in hydrothermalized Pahae natural zeolites: kinetic and isotherm adsorption, and thermodynamics. *Trends in Sciences*, **22**, 8993.

Taddeo R., Prajapati S. & Lepistö R. (2017) Optimizing ammonium adsorption on natural zeolite for wastewaters with high loads of ammonium and solids. *Journal of Porous Materials*, **24**, 1545–1554.

Tang H., Xu X., Wang B., Lv C. & Shi D. (2020) Removal of ammonium from swine waste water using synthesized zeolite from fly ash. *Sustainability*, **12**, 3423.

Tasić Ž.Z., Bogdanović G.D. & Antonijević M.M. (2019) Application of natural zeolite in wastewater treatment: a review. *Journal of Mining and Metallurgy A*, **55**, 67–79.

Teymouri E., Wong K.S., Tan Y.Y. & Mohd Pauzi N.N. (2024) Post-treatment of municipal wastewater using zeolite pervious concrete. *Journal of Water Process Engineering*, **68**, 106408.

United Nations (2015) Transforming our World: The 2030 Agenda for Sustainable Development (A/RES/70/1). United Nations. Available at https://sdgs.un.org/publications/transforming-our-world-2030-agenda-sustainable-development-17981.

Vamvuka D., Loupasis E., Chamilaki E. & Sdoukou E. (2024) Adsorption of ammonium from wastewaters by an almond kernel derived biochar modified by potassium hydroxide or dolomite and activated by steam. *Environmental Advances*, **15**, 100465.

Vezzoli L., Conticelli S., Innocenti F., Landi P., Manetti P., Palladino D.M. & Trigila R. (1987) Stratigraphy of the Latera Volcanic Complex: proposals for a new nomenclature. *Periodico di Mineralogia*, **56**, 89–110.

Wang J. & Guo X. (2020a) Adsorption isotherm models: classification, physical meaning, application and solving method. *Chemosphere*, **258**, 127279.

Wang J. & Guo X. (2020b) Adsorption kinetic models: physical meanings, applications, and solving methods. *Journal of Hazardous Materials*, **390**, 122156.

Wasielewski S., Rott E., Minke R. & Steinmetz H. (2018) Evaluation of different clinoptilolite zeolites as adsorbent for ammonium removal from highly concentrated synthetic wastewater. *Water*, **10**, 584.

Weber J., Walter J. & Morris J.C. (1963) Kinetics of adsorption on carbon from solution. *Journal of the Sanitary Engineering Division*, **89**, 31–59.

Weber T.W. & Chakravorti R.K. (1974) Pore and solid diffusion models for fixed-bed adsorbers. *AIChE Journal*, **20**, 228–238.

Wen D., Ho Y.S. & Tang X. (2006) Comparative sorption kinetic studies of ammonium onto zeolite. *Journal of Hazardous Materials*, **133**, 252–256.

Widiastuti N., Wu H., Ang H.M. & Zhang D. (2011) Removal of ammonium from greywater using natural zeolite. *Desalination*, **277**, 15–23.

Zare K., Sadegh H., Shahryari-Ghoshekandi R. & Asif M. (2016) Equilibrium and kinetic study of ammonium ion adsorption by Fe_3O_4 nanoparticles from aqueous solutions. *Journal of Molecular Liquids*, **213**, 345–350.

Zhou H.D., Wang C.Y., Wang Q., Xu B.X. & Zhu G. (2024) Efficiency, mechanism and application prospect of ammonium adsorption and desorption over a sodium-acetate-modified synthetic zeolite. *RSC Advances*, **14**, 17843–17854.